Emission of terahertz electromagnetic waves from intrinsic Josephson junction arrays embedded in resonance LCR circuits

Masashi Tachiki,* Krsto Ivanovic, and Kazuo Kadowaki
Institute of Material Sciences and Graduate School of Pure and Applied Sciences, University of Tsukuba, Tsukuba 305-8573, Japan

Tomio Koyama
Institute for Materials Research, Tohoku University, Sendai 980-77, Japan
(Received 24 June 2010; revised manuscript received 2 November 2010; published 19 January 2011)

The emission of terahertz electromagnetic waves from an intrinsic Josephson junction array (IJJA) embedded in an *LCR* resonant circuit is studied theoretically. A bias current is applied to the electrodes at the top and bottom of the array. In the voltage state, the ac Josephson current generates a displacement current in the IJJA, and both the currents induce an oscillating current in the electrodes. We describe the whole system, including the array and the environment around it, in terms of an *LCR* resonant circuit. When the Josephson frequency is in the resonance frequency region of the *LCR* circuit, the amplitudes of the displacement current in the Josephson junction array and the oscillating current in the electrodes both are strongly enhanced by a feedback process. We calculate the emission power and the current-voltage (*I-V*) characteristic curve for the system. Inside the frequency region of the *LCR* circuit resonance, stable and intense emission occurs in both the increasing and decreasing processes of the high-bias current. In the emission region the *I-V* characteristic curve has a dip structure. These results are consistent with those of the emission observed in a high-bias current region by using mesa-shaped samples of $Bi_2Sr_2CaCu_2O_{8+\delta}$. We also discuss the difference between the properties of the emission and the *I-V* characteristic curve for intrinsic Josephson junctions embedded in and shunted by the *LCR* resonant circuit.

DOI: 10.1103/PhysRevB.83.014508 PACS number(s): 74.50.+r, 74.25.Gz, 85.25.Cp

I. INTRODUCTION

Since the intrinsic Josephson effects in high-temperature superconductors were first investigated by R. Kleiner and P. Müller, various kinds of new phenomena related to the effects have been found.[1–5] Recently, Ozyuzer *et al.* succeeded in observing the emission of coherent continuous terahertz electromagnetic (TEM) waves from mesa-shaped samples of the high-temperature superconductor $Bi_2Sr_2CaCu_2O_{8+\delta}$ (BSCCO) containing intrinsic Josephson junctions.[6] When the bias current is decreased in the voltage state, an emission is observed near the retrapping point in a region of low bias current.[6,7] The mechanism of this emission is explained in the following way: The ac Josephson current occurring in the voltage state excites a transverse Josephson plasma wave (TJPW). Simultaneously the mesa sample itself works as a resonance cavity, and the amplitude of the resonance mode of the TJPW is enhanced in the cavity. The emission in the low bias-current region was confirmed to be caused by the sample-cavity geometric resonance.[6,7]

Recently, by using samples prepared under different conditions, emission with a different character was observed in a high bias-current region.[8–10] This emission is intense and stable, and it occurs in both the increasing and decreasing processes of the high bias current. The observed TEM wave emission is influenced by the environment around the mesa sample as well as the quality of the sample itself. Therefore, we propose a new mechanism for emission in the region of high bias current. We describe the whole system composed of the BSCCO crystal, the electrodes, and the environment around the sample in terms of inductance *L*, resistance *R*, and capacitance *C*. That is to say, we consider a model of the intrinsic Josephson junction array (IJJA) of BSSCO embedded in an *LCR* resonant circuit.[11] The mechanism of the TEM wave emission from this system is briefly explained as follows: When an external dc current is applied in the direction of the z axis, the ac Josephson current in the voltage state generates an oscillating electric field and thus a displacement current. The Josephson and displacement currents both induce an oscillating surface current in the electrodes. When the frequency of the oscillation is inside the frequency region of the *LCR* circuit resonance, the amplitude of the oscillating current in the electrodes is strongly enhanced by a feedback effect and the oscillating current generates an intense emission of TEM waves, as discussed in Secs. II and III. In the present mechanism for the high bias current, the whole system, including the environment around the BSCCO sample, plays an important role in the emission, different from the sample-cavity geometric resonance of the transverse Josephson plasma in the case of low bias current. In Sec. IV, it is shown that there is an essential difference in the current-voltage characteristic curves between Josephson junction arrays embedded in *LCR* circuits and those shunted by *LCR* circuits.

II. FORMULATION

We formulate equations for calculating the radiation power of the TEM wave and for obtaining the *I-V* characteristic curve. For this purpose we use a model of the IJJA of the BSSCO crystal with electrodes at the top and bottom of the crystal as shown in Fig. 1. A dc current is injected from an external current source.

For this model we set up an equation for the gauge-invariant phase difference of the superconducting order parameter between the neighboring superconducting layers. We write

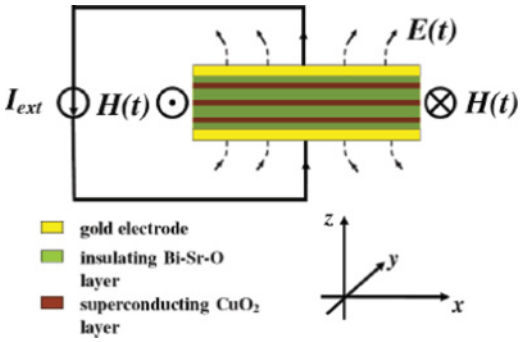

FIG. 1. (Color online) Model of intrinsic Josephson junction array of BSCCO crystal with electrodes. Brown, green, and yellow show the superconducting layers, the insulating layers, and the electrodes, respectively. $E(t)$ and $H(t)$ represent, respectively, the oscillating electric and magnetic fields very near the BSCCO sample with the electrodes.

the phase difference between superconducting layers $l+1$ and l as $P_{l+1,l}$. The inductive and capacitive interactions between the superconducting layers were introduced in Refs. 12 and 13 respectively. Taking account of the interactions and following the calculation procedure given in Refs. 12–16, we obtain the equation for the phase difference:

$$(1-\zeta\Delta^{(2)})\Big[J_c(1-\alpha\Delta^{(2)})\sin P_{l+1,l} + \frac{\hbar\sigma}{2ed}\partial_t P_{l+1,l} + \frac{\hbar\varepsilon}{8\pi ed}\partial_t^2 P_{l+1,l}\Big] = I_{l+1,l}. \quad (1)$$

In Eq. (1), $I_{l+1,l}$ shows the total current density flowing between superconducting layers $l+1$ and l . The first, second, and third terms in the bracket on the left-hand side of Eq. (1) show the contributions from the Josephson, quasiparticle, and displacement current densities, respectively. The variable t and the parameter d indicate, respectively, time and the thickness of the Bi-Sr-O insulating layer in the BSCCO crystal. The parameter J_c denotes the critical current density, and σ and ε, respectively, show the normal conductivity and the dielectric constant along the z axis. The parameters α and ζ indicate, respectively, the capacitive and inductive coupling constants between the superconducting layers, and these parameters are defined as $\alpha = (\varepsilon\mu^2/(sd)$ and $\zeta = \lambda_{ab}^2/(sd)$,$s$ being the thickness of the superconducting layer.[13,15] The parameter λ_{ab} is the penetration depth of the magnetic field applied along the x or y axis, measured from the interface between the BSSCO crystal and the electrode, and μ is the Debye screening length. The operator $\Delta^{(2)}$ is defined as $\Delta^{(2)} f_{l+1,l} = f_{l+2,l+1} - 2f_{l+1,l} + f_{l,l-1}$.

There have been intensive studies on the phase synchronization of conventional Josephson junction arrays shunted by *LCR* circuits.[17–28] In some of the papers the third term in the brackets of Eq. (1) is neglected. In BSCCO crystal the insulating Bi-Sr-oxide layers are much thicker than the superconducting Cu-oxide layers, and the electric polarization in the insulating layers is very large. In this case, the contribution of the displacement current cannot be neglected, and the current plays an important role in phase synchronization. In the region where the Josephson frequencies of the sample are within the frequency width of the *LCR* circuit resonance, the phases are strongly locked[11,23] and $P_{l+1,l}$ can be replaced by P, which is independent of the layers. In this case, if the operators $\zeta D^{(2)}$ and $\alpha D^{(2)}$ operate on the terms in Eq. (1), these terms vanish.

The width L_x of the samples used in the experiments is much narrower than $2\lambda_c$, λ_c being the penetration depth of the magnetic field applied along the y axis and measured from the yz surface. Since the lengths L_x and L_y of the samples used in the experiments are much longer than the height L_z of the samples, the feedback effect due to the electrodes may predominate over the effect of the boundary conditions at the side surfaces. Therefore, we assume that the phase difference P is spatially uniform along the x and y axes. The current $I_{l+1,l}$ in Eq. (1) should be equal to the total surface current density in the electrodes because of the current conservation law; therefore, we can replace $I_{l+1,l}$ by the sum of the external current density $I_{\rm ext}$ and the oscillating surface current density $\partial_t Q/S$ at the electrodes. The quantities Q and S indicate, respectively, the surface charge at the electrodes and the area of the wider surface of the electrodes. Thus, we may approximate Eq. (1) by

$$J_c \sin P + \frac{\hbar\sigma}{2ed}\partial_t P + \frac{\hbar}{2ed}\frac{\varepsilon}{4\pi}\partial_t^2 P = I_{\rm ext} + \frac{\partial_t Q}{S}. \quad (2)$$

The external dc current flows almost uniformly inside the electrodes along the z axis. On the other hand, the oscillating current in the electrodes will flow inside the electrodes or at the side surfaces of the electrodes, depending on whether the thickness of the electrodes is smaller or larger than the penetration depth.

In order to determine the values of P and Q we need another equation. We consider the whole system, which includes the electrodes, the BSCCO crystal, and the environment around the sample, and describe the system in terms of an *LCR* circuit. The charge oscillation induced in the electrodes generates an oscillating voltage between the electrodes. The voltage is composed of the three terms shown on the left-hand side (LHS) of Eq. (3):

$$L\partial_t^2 Q + R\partial_t Q + \frac{Q}{C} = N\frac{\hbar}{2e}\partial_t P + \frac{2}{3}\frac{D^2}{c^3}\partial_t^3 Q. \quad (3)$$

The oscillating currents in the electrodes induce an oscillating magnetic flux in the whole space. The first term on the LHS of Eq. (3) indicates the voltage given by the time derivative of the magnetic flux. The second term on the LHS of Eq. (3) shows the voltage generated by energy dissipation, including dissipation in the electrodes. The charges in the electrodes generate an electric field in the whole space. The third term on the LHS of Eq. (3) expresses the voltage induced by the electric field.

The voltage of the *LCR* circuit should be equal to the sum of the voltage between the top and bottom of the BSCCO crystal and the voltage induced by radiation damping.[29] In Eq. (3), the parameter D indicates the distance between the electrodes, and c is the velocity of light. The first term on the right-hand side (RHS) of Eq. (3) is the voltage generated between the top and bottom of the BSCCO crystal. In this term, $\hbar(2e)^{-1}\partial_t P$ indicates the voltage between the neighboring superconducting layers. N denotes the number of intrinsic Josephson junctions in the BSCCO sample. The second term on the RHS of Eq. (3) denotes the voltage due to radiation damping, which is derived

from the radiation power. Since the total oscillation current is spatially uniform in the sample, the total radiation power emitted from the sample is expressed by use of the dipole emission formula:[29]

$$\text{Radiation power} = \frac{2}{3}\frac{D^2}{c^3}\left\langle\left[\partial_t^2 Q\right]^2\right\rangle_t. \tag{4}$$

In this paper, $\langle A\rangle_t$ denotes the time average of a quantity A.

III. NUMERICAL CALCULATIONS AND RESULTS

We obtain the time dependence of P and Q by numerically solving the coupled Eqs. (2) and (3). For this purpose, we rewrite Eqs. (2) and (3) in terms of nondimensional quantities. The rewritten equations are given by

$$\sin P + \beta\partial_\tau P + \partial_\tau^2 P = i_{\text{ext}} + \partial_\tau q, \tag{5}$$

$$\partial_\tau^2 q + r\partial_\tau q + \omega_{LC}^2 q = \eta\partial_\tau P + \gamma\partial_\tau^3 q. \tag{6}$$

In Eqs. (5) and (6) the nondimensional quantities for t, I_{ext}, and Q (τ, i_{ext}, and q, respectively) and the other parameters are defined as

$$\tau = \omega_p t, \quad i_{\text{ext}} = \frac{I_{\text{ext}}}{J_c}, \quad q = \frac{\omega_p}{SJ_c}Q,$$
$$\beta = \frac{\hbar\omega_p}{2edJ_c}\sigma, \quad r = \frac{R}{L\omega_p}, \quad \omega_{LC} = \frac{1}{\omega_p\sqrt{LC}}, \tag{7}$$
$$\eta = \frac{N\hbar}{2eLSJ_c}, \quad \gamma = \frac{2}{3}\frac{\omega_p}{c^3 L}D^2.$$

In Eq. (7), ω_p denotes the angular frequency of the Josephson plasma at zero wave number. The radiation power [Eq. (4)] is rewritten in terms of nondimensional quantities as

$$\text{Radiation power} = \frac{2}{3}\frac{V^2}{c^3}\omega_p^2 J_c^2\left\langle\left[\partial_\tau^2 q\right]^2\right\rangle_\tau. \tag{8}$$

In Eq. (8), V denotes the volume of the parallelepiped sample.

The values of the parameters in Eqs. (5) and (6) are chosen in the following way: The parameter β is chosen to be 0.1, as shown in Ref. 30. When the calculated radiation power is expressed as a function of the voltage normalized by $\hbar\omega_P/2e$, the half-width of the radiation peak is equal to the value of the resistance r, which depends strongly on the samples and the environment. As a test we take r to be 0.6. The radiation damping constant γ is estimated to be approximately 0.01 by using the expression for γ in Eq. (7) and an approximate value of the inductance L as shown in Ref. 31. We choose a value of 7 for the normalized voltage corresponding to the normalized *LCR* resonant frequency ω_{LC}. We use this value for ω_{LC}, the values for β, r, and γ mentioned earlier, and choose the coupling constant η to be 20. Then, using Eqs. (5) and (6) and the parameter values just described, we calculate the radiation power. Then, we obtain the radiation peak appearing at the external current 0.52 (the external current is normalized by J_c) in the high bias current region. The radiation peak appears in both the increasing and decreasing processes of the external current.

Figure 2 shows the *I-V* characteristic curve. The letter v in Fig. 2 indicates the voltage between the neighboring superconducting layers in the BSCCO crystal. The voltage is normalized by $\hbar\omega_P/2e$, and is equal to the Josephson angular

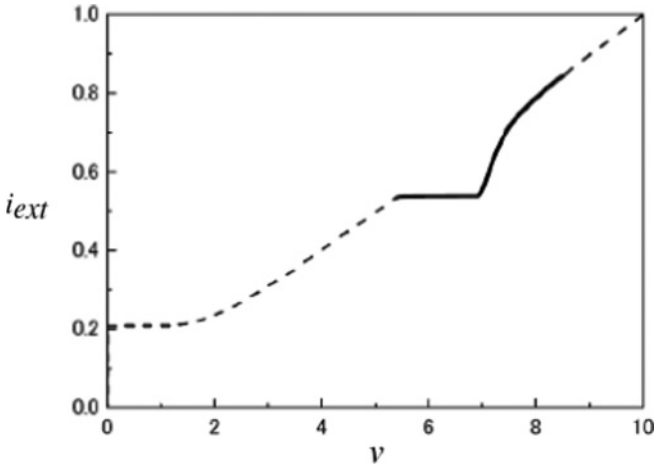

FIG. 2. *I-V* characteristic curve: i_{ext} = external static current density measured in units of critical current density J_c; v = voltage between neighboring superconducting layers, normalized by $\hbar\omega_p/2e$. The solid and dashed lines show the *I-V* curves inside and outside the resonance region, respectively. The parameter values $r = 0.6$, $\omega_{LC} = 7$, $\beta = 0.1$, $\eta = 20$, and $\gamma = 0.01$ are used.

frequency measured in units of the plasma angular frequency ω_p. A dip structure in the *I-V* characteristic curve appears around the normalized voltage $v = 6.98$.

The occurrence of the dip structure is explained as follows: By using Eq. (5) and the energy conservation law, the normalized external current density is expressed as

$$i_{\text{ext}} = i_{\text{ext}}^0 + (1/v)\langle(\beta\partial_\tau P^{\text{os}} - \partial_\tau q)\partial_\tau P^{\text{os}}\rangle_\tau, \tag{9}$$

where i_{ext}^0denotes the external current density in the absence of the *LCR* circuit and P^{os} indicates the oscillating part of the phase difference. The time dependence of $\beta\partial_\tau P^{\text{os}}$and $\partial_\tau q$ at the normalized dip voltage 6.98 is shown in Fig. 3. The amplitude of $\partial_\tau q$ is much larger than that of $\beta\partial_\tau P^{\text{os}}$. Although $\partial_\tau q$ and $\partial_\tau P^{\text{os}}$ do not have the same phase in time, the quantity $\langle\partial_\tau q\partial_\tau P^{\text{os}}\rangle_\tau$ is much larger than $\langle\beta(\partial_\tau P^{\text{os}})^2\rangle_\tau$. From this fact, we see that the second term on the right-hand side of Eq. (9) has negative values in the resonance region of the *LCR* circuit, causing the dip structure in the *I-V* characteristic curve.

The radiation power in units of $2V^2\omega_p^2 J_c^2/(3c^3)$ is shown as a function of the normalized voltage in Fig. 4. We see that the radiation peak appears at a normalized voltage of 6.98. The radiation power at the peak is estimated to be approximately 500 μW for the $100 \times 300 \times 1.5$ μm^3 BSCCO sample.

If the value of the resistivity r is decreased, the half-width of the radiation power becomes smaller and the radiation power at the peak gets stronger. Therefore, to increase the radiation power, we should decrease the load resistance, including the contact resistance. The mechanism of this radiation is explained as follows: As seen in Eq. (8), the radiation power is proportional to the square of the time derivative of the surface current density $\partial_\tau q$ in the electrode. The surface current density is almost equal to the sum of the Josephson current density $\sin P$ and the displacement current density $\partial_\tau^2 P$, since the oscillating normal current density is negligibly small compared with the Josephson and displacement

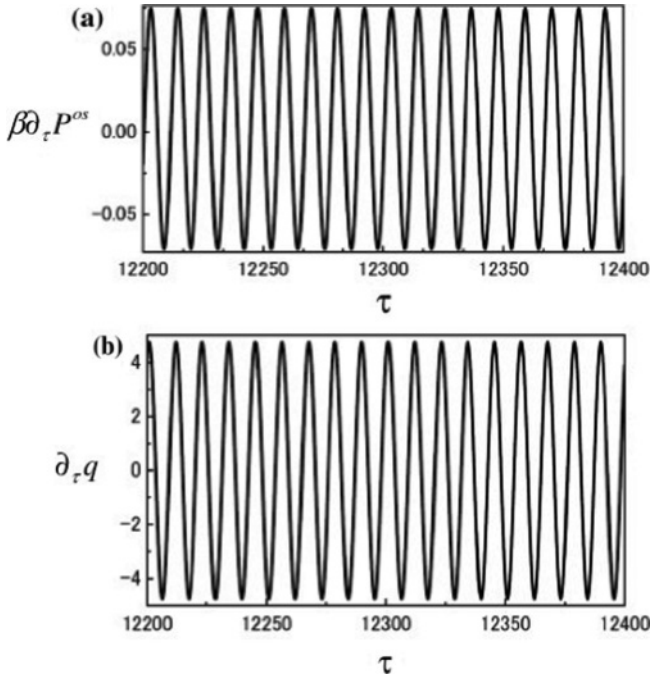

FIG. 3. (a) Time dependence of quasiparticle current density for peak voltage $v = 6.98$; τ denotes ωpt, ωp being the Josephson plasma angular frequency. (b) Time dependence of surface current density in the electrodes at peak voltage $v = 6.98$. All the current densities are normalized by J_c. The values of the parameters are the same as those used in Fig. 2.

current densities. Figures 5(a), 5(b), and 5(c) show the time dependences of the Josephson, displacement, and surface current densities, respectively, at the voltage $v = 5.6$ in the left tail region of the radiation power. As seen in Figs. 5(a) and 5(b), the phases of the Josephson and displacement current densities

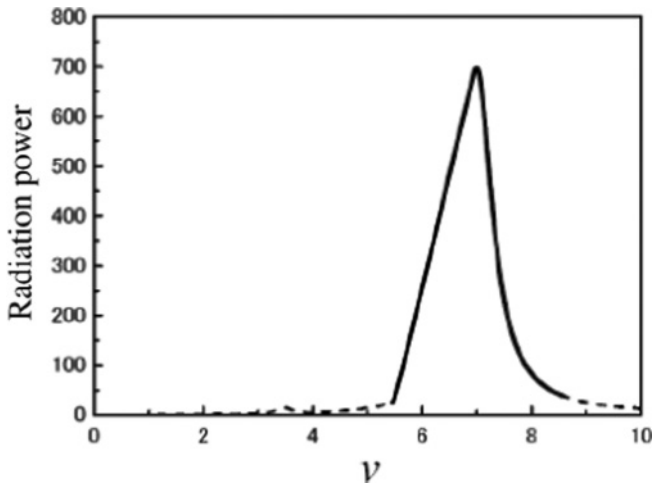

FIG. 4. Radiation power as a function of static voltage. The radiation power is measured in units of $2V^2J_c^2\omega_p^2/(3c^3)$, where V is the volume of the parallelepiped sample. The static voltage is normalized in the same way as in Fig. 2. The solid and dashed lines show the radiation power inside and outside the resonance region, respectively. The values of the parameters are the same as those used in Fig. 2.

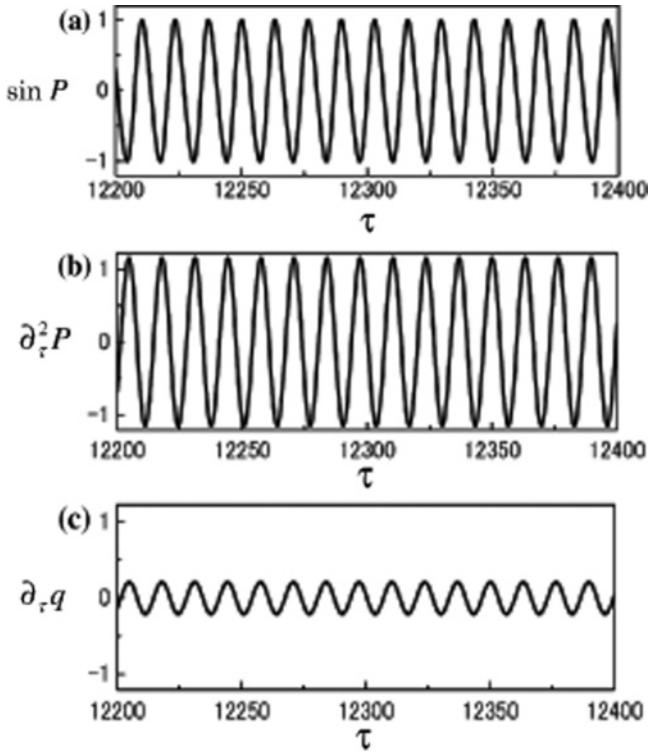

FIG. 5. (a) Time dependence of Josephson current density at voltage $v = 5.6$. (b) Time dependence of displacement current density at the same voltage. (c) Time dependence of surface current density at the same voltage. All the currents densities are normalized by J_c. The values of the parameters are the same as those used in Fig. 2.

are almost out of phase. Therefore, the amplitude of the surface current density is small, as seen in Fig. 5, causing the radiation power to be very weak. When the voltage increases toward that of the radiation peak, the phases gradually get closer to each other and the amplitude of the displacement current increases. When the voltage reaches that of the resonance peak, the phases of the Josephson and displacement current densities are almost in phase and the amplitude of the displacement current density becomes much larger than that of the Josephson current density, as seen in Figs. 6(a) and 6(b). Therefore, the amplitude of the surface current density becomes very large, as shown in Fig. 6(c), and it generates an intensive emission of TEM waves. As discussed earlier, the mechanism of the radiation in a high bias current region differs from that of the radiation caused by the cavity-geometric resonance in a low bias current region. The radiation at the high-bias region occurs in both the increasing and decreasing processes of the bias current.

Figure 7 shows the peak value of the radiation power as a function of the coupling constant η. The values of the other parameters are the same as those in Fig. 2. When the value of η is fixed, the radiation peak appears approximately at the voltage corresponding to the *LCR* resonant frequency ω_{LC}. As shown in Fig. 7, this system starts to radiate TEM waves at approximately $\eta = 1$, and the radiation power at the peak increases as the value of η increases. For large values of η the radiation power drastically increases.

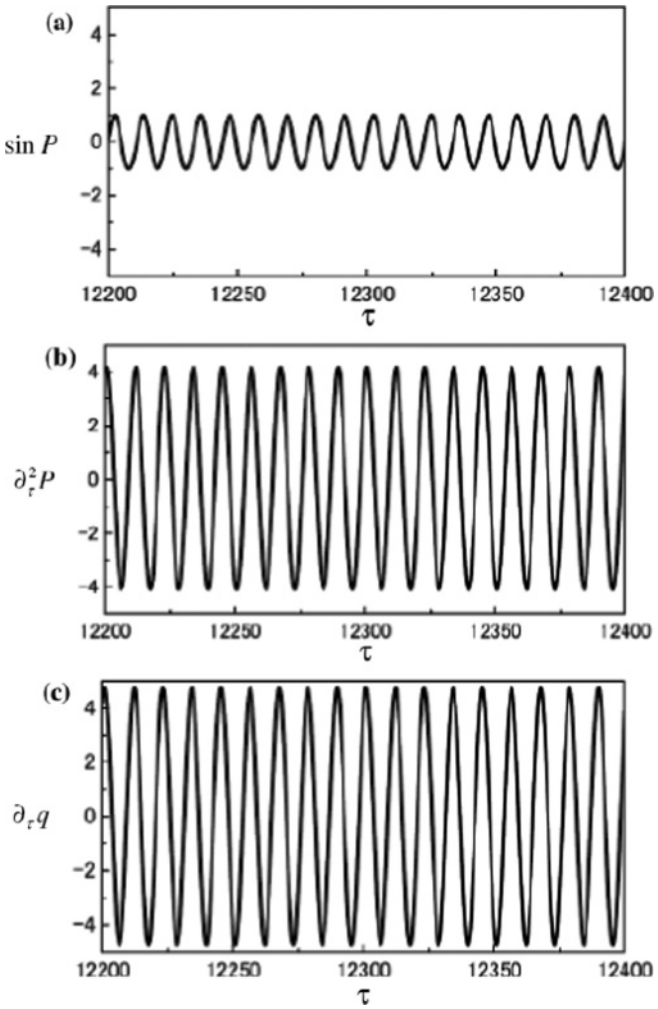

FIG. 6. (a) Time dependence of normalized Josephson current density at peak voltage $v = 6.98$. (b) Time dependence of displacement current density at the same voltage. (c) Time dependence of the surface current density at the same voltage. All the current densities are normalized by J_c. The values of the parameters are the same as those used in Fig. 2.

IV. DISCUSSION AND CONCLUSIONS

In the present study, we use a model in which an array of intrinsic Josephson junctions is embedded in an *LCR* resonant circuit. On the other hand, most studies on synchronization (phase locking) of Josephson junctions have been done by using models of Josephson junction arrays shunted by *LCR* circuits.[17–28,32] Using two-dimensional arrays of Nb/Al/AlO_x/Nb Josephson tunnel junctions, P. Barbara *et al.* observed the strong and coherent emission of 0.15 TEM waves due to phase locking triggered by a resonance in the array structure.[33]

Recently, Zhou *et al.* pointed out that there is an intrinsic difference between the phase-locking properties of a Josephson junction array directly shunted by an *LCR* circuit and an array embedded in the circuit.[11] We show that there is also a remarkable difference between the properties of the *I-V* characteristic curve for these two models. The equations for the array directly shunted by an *LCR* circuit are given just by changing plus signs in front of $\partial_t Q/S$ in Eq. (2) and $\partial_\tau q$ in Eq. (5) to minus signs, and by changing the minus sign in front of $\partial_\tau q$ in Eq. (9) to a plus sign. The sign changes are explained in the following way: In the case of IJJAs embedded in an *LCR* circuit, the current flowing in the BSCCO crystal is equal to the sum of the external current and the oscillating current in the electrodes, as seen in Fig. 1 and discussed in Sec. II. On the other hand, in the case of IJJAs shunted by an *LCR* circuit, the external current is equal to the sum of the currents in the BSCCO crystal and in the *LCR* circuit, as seen in Fig. 8.

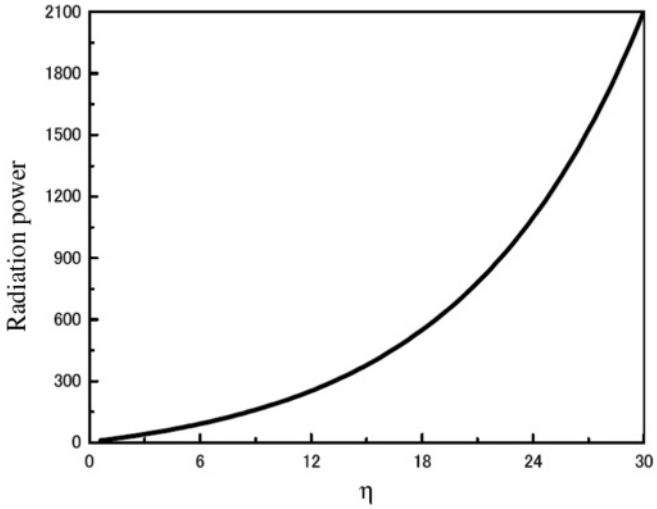

FIG. 7. Radiation power at peak voltage as a function of coupling constant η. The radiation power is normalized as in Fig. 4. The values of the parameters are the same as those used in Fig. 2.

Using the equations for IJJAs shunted by an *LCR* circuit and the parameter values in Fig. 2, we calculate the current-voltage characteristic curve and the radiation power for the system of the Josephson junction array shunted by an *LCR* circuit. The results are shown in Fig. 9. A hump structure appears in the resonance region of the *LCR* circuit, instead of the dip structure in Fig. 2. The appearance of this hump structure is explained as follows: When the minus sign in front of $\partial_\tau q$ in Eq. (9) is changed to a plus sign, the normalized external current for the array shunted by the *LCR* circuit is expressed as $i_{\rm ext} = i_{\rm ext}^0 + (1/v)\langle(\beta\partial_\tau P^{\rm os} + \partial_\tau q)\partial_\tau P^{\rm os}\rangle_\tau$. The second term on the right-hand side of this equation gives a positive contribution to the external current in the voltage region of the *LCR* circuit resonance, causing the hump structure in the *I-V* characteristic

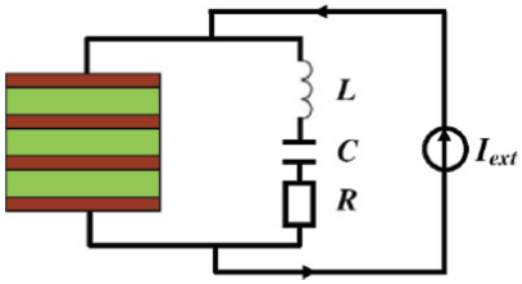

FIG. 8. (Color online) Model of Josephson junction array shunted by *LCR* resonant circuit. Brown and green show superconducting layers and insulating layers, respectively. *L*, *C*, and *R* show the inductance, capacitance, and resistance, respectively, of the external impedance. $I_{\rm ext}$ indicates an external static current density.

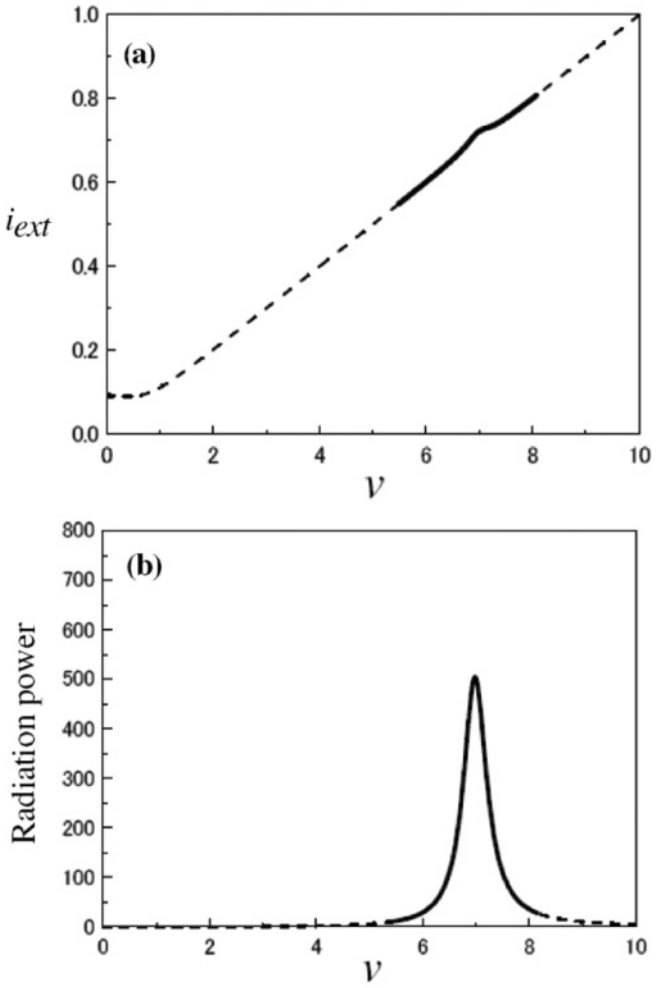

FIG. 9. (a) *I-V* characteristic curve for IJJA shunted by *LCR* circuit. The normalizations of the external current and voltage are the same as in Fig. 2. (b) Radiation power at peak voltage for IJJA shunted by *LCR* circuit as a function of the static voltage. The normalization of the radiation power is the same as in Fig. 4. In Figs. 9(a) and 9(b) the solid and dashed lines show the *I-V* curves and the radiation power, respectively, inside and outside the resonance region. The parameter values are the same as those used in Fig. 2.

curve in Fig. 9(a) As seen in Fig. 9(b), the radiation peak appears very near the normalized voltage corresponding to the normalized resonance frequency of the *LCR* circuit, $\omega_{LC} = 7$. The radiation power at the peak is smaller than that for the array embedded in the *LCR* circuit, shown in Fig. 4. When the coupling constant η is increased from $\eta = 0$, the system starts to radiate TEM waves at approximately $\eta = 1.2$ and the radiation power increases as η increases.

The conclusion of this paper is as follows: When the frequency of the ac Josephson current in the voltage state is inside the frequency region of the *LCR* circuit resonance, the displacement current in the BSCCO crystal is greatly enhanced. The enhanced current generates charge oscillations with a large amplitude in the electrodes. The oscillating charges give rise to an intense emission of TEM waves. The emission occurs in both the increasing and decreasing processes of the high bias current. This behavior of the emission is consistent with experimental results for the high bias current region.[8–10]

When the load resistance is decreased, the width of the emission power with respect to the voltage becomes narrower and the power at the emission peak increases. To obtain this intensive radiation power, it is important to decrease the load resistance, including the contact resistance.

The BSCCO crystals used in experiments are not spatially uniform, and thus the values of the parameters α, ζ, σ, ε, and J_c in Eq. (1) change layer by layer. The inhomogeneity of the parameter values causes a broadening of the radiation frequency width. However, due to the strong phase-locking effect occurring between the superconducting layers, as discussed in Sec. II, the frequency width caused by the inhomogeneity is narrowed compared with the frequency width of the resolution limit of the spectrometers commonly used in the experiments.

In most of the experiments, mesa-shaped samples of BSCCO crystal have been used. Since the thermal conductivity of BSCCO crystals is poor, overheating occurs in the crystal when a high bias current is applied.[34] This may cause an inhomogeneous distribution of temperature in the BSCCO crystals. This heating phenomenon might break the synchronization of the phase differences between the superconducting layers, reducing the radiation power. To avoid heating, it is desirable that samples such as those shown in Fig. 1 be used.

ACKNOWLEDGMENTS

The authors thank R. Kleiner, H. B. Wang, T. Kashiwagi, H. Asai, H. Minami, T. Yamamoto, K. Yamaki, M. Tsujimoto, S. Fukuya, W. Kwok, K. E. Gray, U. Welp, G. Crabtree, V. Vinokur, L. Bulaevskii, A. Koshelev, X. Hu, F. Nori, Y. Nonomura, S. Lin, K. Endo, T. Tachiki, L. Ozyuzer, C. Kurter, H. Matsumoto, and M. Machida for valuable discussions. This work has been supported by the JST (Japan Science and Technology Agency) CREST and the WPI-MANA project.

*tachiki@ims.tsukuba.ac.jp

[1] R. Kleiner, F. Steinmeyer, G. Kunkel, and P. Müller, Phys. Rev. Lett. **68**, 2394 (1992).
[2] R. Kleiner and P. Müller, Phys. Rev. B **49**, 1327 (1994).
[3] K. Lee, W. Wang, I. Iguchi, M. Tachiki, K. Hirata, and T. Mochiku, Phys. Rev. B **61**, 3616 (2000).
[4] V. M. Krasnov, V. A. Oboznov, V. V. Ryazanov, N. Mros, A. Yurgens, and D. Winkler, Phys. Rev. B **61**, 766 (2000).
[5] V. M. Krasnov, T. Bauch, and P. Delsing, Phys. Rev. B **72**, 012512 (2005).
[6] L. Ozyuzer *et al.*, Science **318**, 1291 (2007).
[7] M. Tsujimoto, K. Yamaki, K. Deguchi, T. Yamamoto, T. Kashiwagi, H. Minami, M. Tachiki, K. Kadowaki, and R. A. Klemm, Phys. Rev. Lett. **105**, 037005 (2010).
[8] K. Kadowaki *et al.*, Physica C **468**, 634 (2008).
[9] H. Minami, N. Orita, T. Koike, T. Yamamoto, and K. Kadowaki, Physica C **470**, S822 (2010).
[10] H. B. Wang *et al.*, Phys. Rev. Lett. **105**, 057002 (2010).
[11] T. Zhou, J. Mao, H. Cui, X. Zhao, L. Fang, and S. Yan, Physica C **469**, 785 (2009).

[12]S. Sakai, P. Bodin, and N. F. Pedersen, J. Appl. Phys. **73**, 2411 (1993).
[13]T. Koyama and M. Tachiki, Phys. Rev. B **54**, 16183 (1996).
[14]See M. Tachiki, T. Koyama, and S. Takahashi, in *Coherence in High Temperature Superconductors*, edited by G. Deutscher and A. Revcolevschi (World Scientific, Singapore, 1996), p. 371.
[15]M. Tachiki, M. Iizuka, K. Minami, S. Tejima, and H. Nakamura, Phys. Rev. B **71**, 134515 (2005).
[16]F. Marchesoni, S. Savel'ev, M. Tachiki, and F. Nori, Phys. Rev. B **81**, 174531 (2010).
[17]P. Hadley and M. R. Beasley, Appl. Phys. Lett. **50**, 621 (1987).
[18]P. Hadley, M. R. Beasley, and K. Wiesenfeld, Phys. Rev. B **38**, 8712 (1988).
[19]A. A. Chernikov and G. Schmidt, Phys. Rev. E **52**, 3415 (1995).
[20]K. Wiesenfeld and J. W. Swift, Phys. Rev. E **51**, 1020 (1995).
[21]K. Wiesenfeld, P. Colet, and S. H. Strogatz, Phys. Rev. Lett. **76**, 404 (1996).
[22]A. B. Cawthorne, C. B. Whan, and C. J. Lobb, J. Appl. Phys. **84**, 1126 (1998).
[23]G. Filatrella, N. F. Pedersen, and K. Wiesenfeld, Phys. Rev. E **61**, 2513 (2000).
[24]A. N. Grib, P. Seidel, and J. Scherbel, Phys. Rev. B **65**, 094508 (2002).
[25]G. Filatrella, N. F. Pedersen, C. J. Lobb, and P. Barbara, Eur. Phys. J. B **34**, 3 (2003).
[26]S. Madsen, G. Filatrella, and N. F. Pedersen, Eur. Phys. J. B **40**, 209 (2004).
[27]N. F. Pedersen and S. Madsen, Supercond. Sci. Technol. **20**, S1 (2007).
[28]S. Madsen, N. Grønbech-Jensen, N. F. Pedersen, and P. L. Christiansen, Phys. Rev. B **78**, 174525 (2008).
[29]See J. R. Oppenheimer's, *Lectures on Electrodynamics*, edited by Elliot W. Montroll, George H. Vineyard, and Maurice Lévy (Gordon and Breach, New York, 1970), p. 76.
[30]Using the parameter values $v_p = 100-300$ GHz, $J_c = 107$ A/m^2, and $\sigma = 4$ S/m [Y. I. Latyshev, A. E. Koshelev, and L. N. Bulaevskii, Phys. Rev. B **68**, 134504 (2003)], we estimate the values for $\beta = 0.07-0.21$, and choose $\beta = 0.1$ in this paper.
[31]In estimating the parameter γ, we use the relation in Eq. (1) and the inductance $L = D/c^2$. The expression for the inductance is an approximate one since it is valid when the length of the conducting wire is much larger than the diameter.
[32]I. Martin, G. B. Halász, L. N. Bulaevskii, and A. E. Koshelev, J. Appl. Phys. **108**, 033908 (2010).
[33]P. Barbara, A. B. Cawthorne, S. V. Shitov, and C. J. Lobb, Phys. Rev. Lett. **82**, 1963 (1999).
[34]C. Kurter *et al.*, IEEE Trans. Appl. Supercond. **19**, 428 (2009).